Biol. Cybern. 70, 569–578 (1994)

Biological Cybernetics

Bistability and the dynamics of periodically forced sensory neurons

André Longtin [1], **Adi Bulsara** [2], **David Pierson** [3], **Frank Moss** [3]

[1] Département de Physique, University of Ottawa, 150 Louis Pasteur, Ottawa, Ont., Canada K1N 6N5
[2] NCCOSC–RDT&E Division, Materials Research Branch, San Diego, CA 92152, USA
[3] Department of Physics, University of Missouri at St. Louis, St. Louis, MO 63121, USA

Received: 22 March 1993/Accepted in revised form: 8 September 1993

Abstract. Many neurons at the sensory periphery receive periodic input, and their activity exhibits entrainment to this input in the form of a preferred phase for firing. This article describes a modeling study of neurons which skip a random number of cycles of the stimulus between firings over a large range of input intensities. This behavior was investigated using analog and digital simulations of the motion of a particle in a double-well with noise and sinusoidal forcing. Well residence-time distributions were found to exhibit the main features of the interspike interval histograms (ISIH) measured on real sensory neurons. The conditions under which it is useful to view neurons as simple bistable systems subject to noise are examined by identifying the features of the data which are expected to arise for such systems. This approach is complementary to previous studies of such data based, e.g., on nonhomogeneous point processes. Apart from looking at models which form the backbone of excitable models, our work allows us to speculate on the role that stochastic resonance, which can arise in this context, may play in the transmission of sensory information.

1 Introduction

This article examines the conditions under which periodically stimulated neurons can be modeled as bistable systems embedded in noise. The motivation for this work lies in experimental studies of phase locking in neurons of various sensory modalities. The auditory fibers of the squirrel monkey (Rose et al. 1967) and of the cat (Kiang 1984), cat retinal ganglion cells (Ogawa et al. 1966) and primary visual cortex (Siegel 1990), and mechanoreceptors of the macaque monkey (Talbot et al. 1968) are examples of cells which exhibit multimodal interspike interval histograms (ISIHs) when subjected to periodic forcing. The peaks of these ISIHs are located at integer multiples of the driving period T_0 and, except for the first few peaks, the envelope of the ISIH decays exponentially. Further, this behaviour is often seen across a large range of stimulus intensities. Apart from the phase preference, the firing of action potentials in these systems is aperiodic, as a random number of stimulus cycles can be 'skipped' between successive spikes.

Modeling of this kind of spike activity has focussed primarily on stochastic point processes (especially in the auditory literature: see, e.g., Weiss 1966; Johnson 1974; Kiang 1984; Gummer 1991; Lowen and Teich 1992). In the presence of a time-varying stimulus, these model processes are typically nonhomogeneous, i.e., their instantaneous rate is time-dependent (see Tuckwell 1989 for a review of stochastic modeling). Although these models can account for many features of the data, they do not have a spiking mechanism per se, as do the Hodgkin-Huxley equations and other excitable models. Recently, these ISIH data have been shown to be similar in many respects to histograms of residence times in the wells of noisy bistable systems (Fig. 1a) with periodic forcing (Longtin et al. 1991). Such potentials have been used to model a wide variety of systems, including the channel dynamics of auditory hair cells (Corey and Hudspeth 1983). Noisy bistable models have a long history in the fields of neural modeling and neural networks, especially as a powerful conceptual tool (Landahl et al. 1943; Hopfield 1982). Apart from being relevant for the study of genuinely bistable neural dynamics (see Sect. 3), they form the backbone of many excitable models. The "noisy bistability" point of view can help bridge the gap between point-process and excitable models, e.g., by allowing one to investigate how noise is coupled to the excitable dynamics. Further, this point of view raises the following question which is addressed in this article. What aspects of the data are due to the statistical properties of noisy two-state systems? This description could further benefit from the extensive literature on periodically forced noisy bistable systems (see, e.g., McNamara and Wiesenfeld 1989). It can shed new light on the mechanisms of sensory encoding and on a positive role for noise, traditionally known for, e.g., imposing limits on stimulus discrimination

Correspondence to: A. Longtin

(Siebert 1965). In particular, it is a highly exciting possibility that signal amplification by noise, an effect known as stochastic resonance (SR) (see Sect. 3), may play a role at different stages along afferent sensory pathways. While our study does not focus on this effect, it does lay the ground work for exploring SR in real neural systems. Recent work has in fact shown that excitable systems can exhibit SR (Chialvo and Apkarian 1993; Douglass et al. 1993; Longtin 1993), and the present work focusses on the related class of bistable models, which are simpler (and thus more tractable), yet still biologically relevant.

Section 2 gives a brief review of the existing literature on stochastic phase-locking. Section 3 presents the bistable models of interest and elaborates on aspects of the theory of periodically forced bistable systems which are useful to understand the skipping phenomenon. Analog computer simulations of the standard quartic and neuron models are presented in Sect. 4. They are compared to recently obtained cat auditory nerve data to illustrate how easily bistable models can reproduce the major statistical and temporal features of the data. Section 5 is a numerical study of a bistable model with 'soft potential' which examines the effects of noise bandwidth on ISIHs and return maps, as well as the amplitude dependence of the ISIH decay rate. The article closes with a discussion in Sect. 6.

2 Background

To our knowledge, the earliest attempt to model the skipping phenomenon can be found in the seminal work of Gerstein and Mandelbrot (1964). Their random walk integrate-and-fire (IF) model could generate peaks at integer multiples of the driving period when the parameter controlling the deterministic drift toward threshold was periodically modulated, simulating the action of auditory tone bursts (clicks) on the auditory fibers. Weiss (1966) has also proposed, as part of a model of the auditory periphery, a model neuron (intended to represent VIIIth nerve neurons) which is driven by the output of the transducer (i.e., the hair cell generator potential) as well as by gaussian noise. This model has a refractory period but no spiking mechanism per se (i.e., it is an IF model). It reproduces some of the features of multimodal ISIHs in response to fast auditory clicks (≈ 0.1 ms) presented at a slow rate. The intervals between peaks were determined by the oscillatory impulse response functions of the cochlear partition at the location of the hair cell which connects to the fiber. Below we focus on a general simple model of sensory neurons with sinusoidal stimulation (rather than periodic clicks) at various driving periods (greater than the refractory period) where skipping is observed. The phase-locking dynamics of biological oscillators has attracted much attention, especially when a steady entrainment pattern (e.g., m firings occurring during n cycles of the stimulus) is observed experimentally. However, Glass et al. (1980) have studied the phase-locking dynamics of a simple IF model with noise and have found unstable zones with no phase-locking in between regions of phase space with stable phase-locking patterns. For low-amplitude periodic inputs, their model yielded quasi-periodic dynamics, while patterns with irregular skipped or intercalated beats were seen at higher amplitudes.

Another popular approach involves estimating the parameters of a stochastic point-process model to reproduce statistics of first order (such as the ISIH) and higher. Point processes in which the instantaneous rate is a fractal noise (Lowen and Teich 1992) are able to further account for slight correlations between spikes (i.e., "nonrenewability") which have been hypothesized to underlie spike clustering in spontaneous and driven auditory nerve data from certain species. The pure tone case has received special attention in the auditory literature and has led to the definition of an index of synchronization of the spiking to a harmonic of the stimulus (Johnson 1974). Modulation of a point process leads to time-dependent transition rates (ie., nonhomogeneity); yet it remains a Poisson point process as long as the spontaneous or modulation-induced transition rates between the states of the underlying system are slower than the internal relaxation times of the system. In this sense, the bistable models below generate switching events which obey the statistics of nonhomogeneous Poisson point processes (except for slight memory effects, see Sect. 4). A complementary approach to stochastic point processes lies in recent work on stochastic neural models incorporating a spiking mechanism to reproduce, e.g., current-firing rate characteristics (see, e.g., Treutlein and Schulten 1985). These models involve stochastic differential equations and thus have a deterministic component. This is interesting because, for certain data (e.g., Talbot et al. 1968), deterministic phase-locking can be seen at higher frequencies, suggesting an interplay between deterministic and stochastic processes.

3 The model

We focus on systems in the limit of large damping (which makes the acceleration term negligible) governed by the equation

$$\frac{dx}{dt} = -\frac{dU(x)}{dx} + \xi(t) + \varepsilon \sin(\omega t) \tag{1}$$

where $U(x)$ is a double-well potential (Fig. 1a) and $\xi(t)$ is a gaussian-distributed white noise process of zero mean. White noise has a flat power spectrum; its autocorrelation is given by $\langle \xi(t)\xi(s) \rangle = 2D\delta(t-s)$. For our purposes here, the state variable $x(t)$ can be viewed as the soma potential. The right-hand side is the sum of all the forces acting on the "particle": the force arising from the potential $U(x)$, the modulation force and the stochastic force. Intuitively, the relaxation rate back to the resting potential is proportional to the steepness of the slope of the potential in the vicinity of the state identified with the resting state. Various approximate analytical expressions have been obtained (Zhou et al. 1990) for the distribution of residence times T (Fig. 1b) within a given well. This approach is interesting because it relates ISIH features

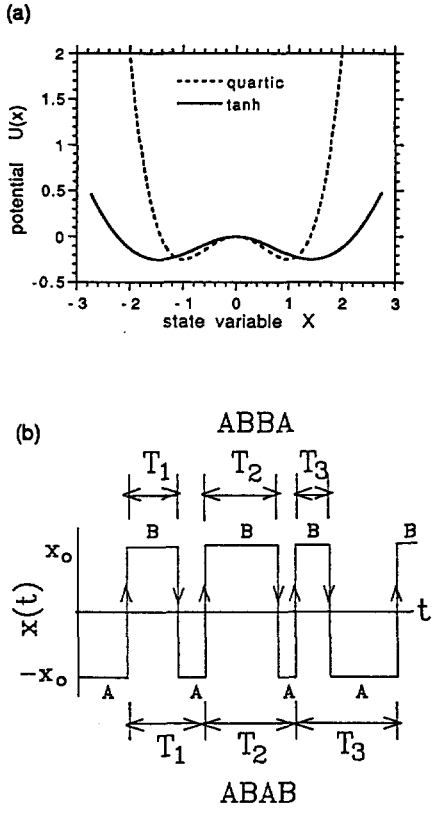

Fig. 1. **a** Double-well potentials used in our study: hyperbolic tangent (*solid line*) and standard quartic (*dotted line*). State A corresponds to $x(t) < 0$, and state B to $x(t) > 0$. **b** Signal obtained by applying a two-state filter to the time series corresponding to a particular realization of the stochastic process given by (1). The two symmetries of interest refer to ABBA events (*upper labels*) and ABAB events (*lower labels*). Equation (4) was used with a stimulus period of 4

(widths of peaks, etc.) to basic parameters of the 'potential' in which the soma voltage evolves. This theory further has the advantage over certain point-process models of always yielding positive probability values.

Although the identification of 'states' in the model with those of the neural system is not obvious, we expect that the eventual significance of our results will not depend on such a precise identification. One can readily identify the resting state of the neuron with the equilibrium point of the left well (Fig. 1a) as both are stable in the absence of forcing (the neurons of interest here fire spontaneously and randomly in the absence of forcing). The other state may correspond to an excited state (above threshold, with or without repetitive firing) which does not immediately reset to the resting state (certain excitable cells are known to exhibit such "long plateaus", see Rinzel and Ermentrout 1989); alternatively, it may correspond to a recovery state characterized by hyperpolarization, due either to the intrinsic ionic current dynamics of the cell or to the effect of inputs from other neurons, or both. In either case, the model assumes a stochastic reset from this state back to the resting state. It should be mentioned that our results are qualitatively similar when the reset has a weak or strong deterministic component (the latter occurring in excitable models: see, e.g., Chialvo and Apkarian 1993; Douglass et al. 1993; Longtin 1993). An excitable cell such as a neuron has a characteristic current-voltage relation which is N-shaped (see, e.g., Rinzel and Ermentrout 1989), as does the negative gradient of a bistable potential; in other words, the N-shaped nonlinearity we investigated can be viewed as the backbone of excitability. While this fact in itself justifies our study of (1), it is important to note that bistability of various forms has been observed in simplified Hodgkin-Huxley-type neuron models as well as in vivo (see Rinzel and Ermentrout 1989 for a review). For example, bistability between a fixed point (no spiking) and a limit cycle (periodic spiking) in the squid giant axon has been observed. Bistability between two fixed points has also been found in models. It is possible, thus, that the main features of the data, and in particular signal enhancement by noise, are captured by the bistability feature per se, regardless of the kinds of states involved. For example, multimodal ISIHs could arise when noise kicks the system between a fixed point and a low-frequency limit cycle (it is thus likely that only one firing would be observed during a mean residence time on the limit cycle).

In this article, the "standard quartic model" and the Schmitt trigger are studied using simulations on an analog computer, while the softer potential of the "neuron model" is studied via both analog and digital simulations. The neuron model is described by the following nonlinear dynamic equation for the membrane potential $x(t)$:

$$\dot{x} = -ax + b\tanh x + F(t) + \varepsilon \sin \omega t \tag{2}$$

We now assume (and from now on), however, that $F(t)$ is a zero mean gaussian noise with finite spectral bandwidth, i.e., with non-zero correlation time τ_c (equal to the inverse of its bandwidth). Its autocorrelation is $\langle F(t)F(s)\rangle = \frac{D}{\tau_c}\exp(-|t-s|/\tau_c)$, and its variance is simply D/τ_c. In the limit $\tau_c \to 0$ we recover gaussian delta-correlated noise (i.e., white noise) with variance $2D$. The stochastic process $F(t)$ (known as an Ornstein-Uhlenbeck process) is governed by $\frac{dF}{dt} = -\lambda F(t) + \lambda\xi(t)$ where $\lambda^{-1} \equiv \tau_c$. In the analog simulations below, $F(t)$ is generated by low-pass filtering quasi-white noise from a noise generator, the resulting bandwidth being equal to λ. The stochastic numerical simulations reported below were carried out using the algorithm of Manella and Palleschi (1989).

The potential function corresponding to the flow in (2) is shown in Fig. 1a. The barrier maximum is at $x = 0$ and the minima are located at $c \approx \pm b\tanh(b)$, the approximation holding for large b (we set $a = 1$ throughout this work). The potential is bistable for $b > 1$. When the mean residence time (for $\varepsilon = 0$) in a stable steady state is long compared with the internal relaxation time within the wells (local equilibrium assumption), and the noise is white and of low intensity, the rate of interwell switching is well described by the Kramer's rate (see Gardiner 1983)

$$r_0 \approx (2\pi)^{-1}[\,|U^{(2)}(O)|\,U^{(2)}(c)]\exp(-U_0/D) \tag{3}$$

where U_0 is the height of the potential barrier and $U^{(2)}(x) \equiv d^2U/dx^2$. Kramer's rate is found to decrease monotonically with increasing τ_c (Jung et al. 1989). When $D = 0$, interwell transitions are coherent with harmonic driving only if ε is sufficiently large. In the presence of both noise and modulation, the transition rates become time-dependent, due to the raising and lowering of the wells with respect to the barrier. A logical extension of Kramer's theory to this case has led to postulating (when $\varepsilon \ll U_0$ and $\omega < r_0$; see, e.g., McNamara and Wiesenfeld 1989) a Kramer's rate given by (3) with U_0 replaced by $U_0 + \varepsilon \sin\omega t$. An effect known as 'stochastic resonance' (SR) occurs when the r_0 is commensurate with the switching rate imposed by the external forcing, even though this forcing by itself cannot produce switchings (McNamara and Wiesenfeld 1989). The particle then has a high probability of switching at each stimulus half-cycle, i.e., the switchings correlate highly with the modulation. The signal-to-noise ratio (SNR) of $x(t)$ measured at ω exhibits a maximum ("resonance") as a function of D. SR thus leads to the counter intuitive notion that adding noise can enhance the observability of the impressed signal. The switching dynamics can also be studied using the distributions of residence times in the wells (or, equivalently, of transition times between wells). A resonance appears as the peak heights go through maxima as a function of D (Zhou et al. 1990); this has been linked to SR, although the matching of the aforementioned time scales has not yet been clearly established. It is an interesting prospect that SR is at work helping the sensory neurons respond to weak periodic signals. We did not study SR here even though it is a property (Bulsara et al. 1991) of the bistable models which, we will show, fit the data so well.

4 Analog simulations

Electronic analog computation is much faster than digital computation for studying stochastic problems. Further, analog computers are "real systems" with their own imperfections and nonlinearities, and their behavior can be seen as generic. This section discusses analog simulations of (2) as well as of the dynamics of the 'standard quartic' potential $U(x) = -\frac{x^2}{2} + \frac{x^4}{4}$:

$$\dot{x} = x - x^3 + F(t) + \varepsilon \sin(\omega t) \tag{4}$$

Here $U(x)$ (Fig. 1a) has a barrier height $U_0 = 1/4$ and minima located at $c = \pm 1.0$. The design and operation of these simulators have been described previously (Bulsara et al. 1991). The Schmitt trigger has also been used in a preliminary study of these ISIH data (Longtin et al. 1991). The "neuron" model of (2) is a "soft" potential, since it goes to infinity linearly in x. The standard quartic is "harder" , going to infinity as x^4, while the Schmitt trigger can be seen as a potential with infinitely hard walls located at thresholds $\pm c$. Our goal is to show that while these three potentials are radically different as regards their stiffness, they are able to satisfactorily reproduce the ISIH data. The conclusion to be drawn from this observation is that matching physiological data to such model potentials is not likely to reveal much about the "potentials" in which the soma voltage evolves. However, that the observed behaviors of real neurons are so easily mimicked by such simple bistable models strongly suggests that their dominant characteristics are describable by two-state dynamics.

Let AB represent a transition of the system state point from well A to well B. A time interval between an AB event and its following BA "reset" event will be referred to as an ABBA event (Fig. 1b). Such intervals are the statistical escape times from well B. One can, as we do below, assemble these escape times (or "residence times") into a histogram called the "probability density of escape times" or the "residence time histogram". Such a histogram has been previously investigated for (4) both theoretically and with analog and digital simulations (Zhou et al. 1990). It was found that the ABBA symmetry leads to a series of peaks in the escape time probability density located at the odd integer multiples of $T_0/2$. A time interval between an AB event and the next AB event, ignoring the time of the reset event BA, will be referred to as an ABAB event. Here the escape times from both wells are involved. The total escape time is not, because of memory effects, simply the sum of the two independently determined escape times. Nor is the peak sequence the same. This symmetry leads to a sequence of peaks in the probability of escape times located at all integer multiples of T_0 (Longtin et al. 1991). In the physiological data only the ABAB sequence is observed, since ISIs are the times between sequential firing events. The reset event, which can be associated with membrane repolarization, is hidden from this measurement. Thus, only the ABAB symmetry is experimentally accessible. In the following, only the ABAB symmetry is used.

4.1 Aligning model and observed ISIHs

The probability density of ABBA escape times from a bistable system is well approximated by a gamma-like distribution

$$P(T) = \frac{T}{\langle T \rangle^2} \exp - \frac{T}{\langle T \rangle} \tag{5}$$

where $\langle T \rangle$ is the mean time spent in one well. The major features of the gamma distribution are $\lim_{T \to 0} P(T) = 0$, and $\lim_{T \to \infty} P(T) \simeq exp(-T/\langle T \rangle)$. The density of ABAB events also has this general form, as do spontaneous ISIHs from those cells which exhibit multimodal ISIHs in the presence of a stimulus. One limiting case of this distribution is the decaying exponential which is the theoretical distribution of escape times for the "random telegraph signal" (which is derived from a Poisson point process, see Gardiner 1983). This density is approximated by the escape time distribution (for both symmetries) when $\tau_c \to 0$, and the switching time between the wells is short compared with $\langle T \rangle$. In analog simulations, the switching time is determined by the integration time constant τ_i (i.e., the actual coefficient of $\dot{x}$ in (2) and (4),

determined by the RC value of the electronic integrator), while $\langle T \rangle$ is mainly determined by $U(x)$.

Figure 2a shows an ISIH obtained from the primary auditory nerve of a cat with an 800 Hz, 60 dB sound pressure level (SPL) stimulus to the ear. We note the sequence of decaying peaks located at all integer multiples of $T_0 \equiv 1.25$ ms characteristic of the ABAB symmetry. Figure 2c shows an analog simulation of the physiological data at 800 Hz, using the standard quartic (solid line) and the "neuron" [(2), dashed line] potentials. What is remarkable is that only one adjustable parameter is necessary to fit the experimental data. We can adjust either D or ε, save only that the other parameter lies within some range not very different from the barrier height U_0. If we had plotted the simulated ISIHs on top of the physiological data, the three curves would have become indistinguishable. We note, however, that the value $\tau_i = 10^{-4}$ in the circuit is of the same order of magnitude as a neural membrane time constant, e.g., 0.3–0.8 ms for guinea pig inner hair cells as measured by Russell and Sellick (1978) (hair cells produce the "receptor potential" which induces the action potential in the postsynaptic axon from which the spikes trains are recorded). If τ_i were different by a few orders of magnitude, the fits would not be as good. Further, the noise used in these simulations has a correlation time of at most 0.1 τ_i, simulating the typically higher bandwidth of membrane noise or input noise (Calvin and Stevens 1968).

4.2 Nonmonotonicity of the ISIH envelope

When the stimulus intensity is small or its frequency high, the first peak of the ISIH is not the highest, as shown in Fig. 2b (Rose et al. 1967; Talbot et al. 1968). This represents cat auditory data at 800 Hz as in Fig. 2a, but at the weaker sound intensity of 30 dB SPL. The second peak is the highest, and the decay of the ISIH envelope is exponential after the third peak (not shown). Figure 2d shows that this effect is also exhibited by our bistable analog simulators when ε or D are reduced from their values in Fig. 2c. Once again, the analog results lie virtually on top of the neurophysiological data (not

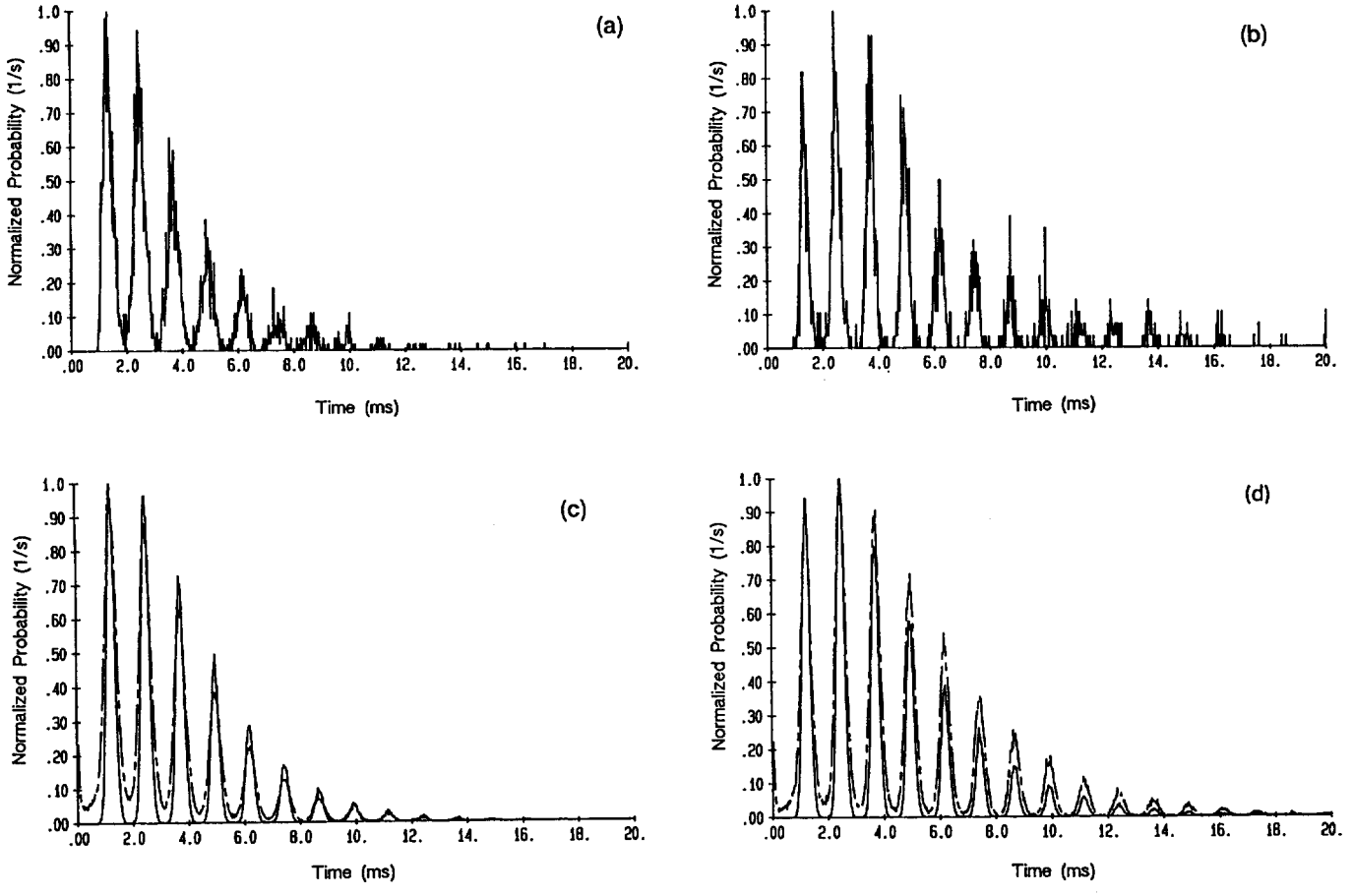

Fig. 2. Experimental interspike interval histogram (ISIH) data from cat primary auditory nerve with an 800-Hz stimulus: 60 dB SPL (**a**) and 30 dB SPL (**b**) (after Rhode). **c**. ISIHs from analog simulations at 800 Hz: the standard quartic with $\varepsilon = 0.209$ V and $2D = 0.0576$ V^2 (*solid line*) and the neuron model with $\varepsilon = 0.209$ V and $2D = 0.0756$ V^2 (*broken line*). The noise intensities have been adjusted to achieve the fits and are different because the barrier heights of the two potentials are different. Note that D was changed rather than ε, as both play similar roles: see Fig. 4. **d**. Analog simulations in the reduced amplitude case corresponding to **b**. The parameters for the standard quartic (*solid line*) are $\varepsilon = 0.209$ V and $2D = 0.0425$ V^2, and for the neuron model (*broken line*), $\varepsilon = 0.209$ V and $2D = 0.0602$ V^2. The integration time constant is $\tau_i = 10^{-4}$ and $\tau_c = 10^{-5}$

shown). While it is tempting to associate this nonmonotonicity with nonrenewability, one must remember that a renewal process can have any ISIH. The following discussion illustrates this point in the context of simple models of skipping.

The nonmonotonicity of the residence time density occurs in both the ABBA and ABAB sequences but is more evident in the latter (and is minimized for the ABBA sequence if the noise is white, as explained earlier in Sect. 4). It can be understood on simple statistical grounds. For a bistable system with periodic modulation, let us denote by p the probability of an AB transition during the half of the modulation period where this transition is favored (the probability of a BA transition during the other half being also p). Then the probability of an AB transition during the ith cycle of the stimulus (since the last BA event) is

$$P_i(AB) = p(1-p)^{i-1} \tag{6}$$

The probability of an ABAB event being complete after the ith cycle is given by

$$P_i(ABAB) = p^2 i(1-p)^{i-1} \tag{7}$$

This follows from (6) because an extra BA event (of probability p) is required; the factor i accounts for the different possible times at which the first AB transition can occur. Also, $\ln P_i(ABAB)$ does not depend linearly on i for small i, due to the factor $(\ln i)$. However, after the first few spikes, (7) does indeed become linear in i on a logarithmic scale, since the $(1-p)^{i-1}$ factor dominates. In this simple model, (6) is a straight line on a log-lin scale, as in Zhou et al. (1990). This simple model also predicts that the maximum of the ISIH occurs at $i_{\max} = -[\ln(1-p)]^{-1}$. Thus, as $p \to 0$, $i_{\max} \to \infty$; and as $p \to 1$, $i_{\max} \to 0$. This is observed in neural data and our simulations: as the amplitude increases, p increases, and the probability shifts towards the first peaks. The proper behavior as a function of frequency also ensues by making p proportional to the stimulus period. Note that in this description the process is still considered renewal, since the probability p does not depend on i, the cycle number. The nonmonotonicity can thus arise from the simple statistics of counting the two events that make up an ABAB event.

It is also conceivable that a nonrenewal process underlies the nonmonotonicity. This would not be surprising given that correlations are suspected to account for the cluster shapes the return maps (Sect. 5). For example, the firing probability during one cycle might depend upon the last firing time. This is evident if one considers an even simpler model of the skipping behavior, in which p is now the probability of a "firing" (or completion of an ABAB event) occurring during a given cycle of the stimulus. Then the probability of firing in the ith cycle since the last firing is given by $P_i = p(1-p)^{i-1}$, for which $\ln P_i = ai + b$ where a, b are constants. In this model, exponential decay is a signature of the independence of successive firing events, and nonmonotonicity arises only when $p = p(i)$, i.e., when p depends on the cycle number (the constants a and b could now depend on i). But here there is only one way to fire after i cycles, while in the preceeding discussion, nonmonotonicity arose because of the multiple ways to make up a "firing after i cycles" event. In the present picture where p has a memory of past cycles, each successive cycle of the stimulus brings the soma voltage closer to crossing the metastable point, until finally one cycle kicks it over. This image is helpful when the frequency of the modulation is too high or the amplitude is too low; in both cases, the "particle" does not have time to exit on the first cycle. It is probable that some aspects of the nonmonotonicity can be understood in terms of renewal processes, and others in terms of memory effects. In fact, it seems that (7) may apply to a genuinely bistable neuron, while this last model (for which nonexponential decay implies ISI correlation) may be more appropriate for IF or excitable dynamics (or any with a large deterministic reset component).

5 Return maps, noise, and scaling

We now discuss in greater detail the finer aspects of the ISIHs. The numerical simulations in this section are of (2) with $b = 1.6056$ corresponding to a barrier height $U_0 = 0.25$ and minima located at ± 1.44. The range of signal and noise intensities must be appropriately selected in order to obtain a well-defined ISIH peak sequence. Too high a noise intensity will destroy the peak structure, leading to a single large peak with a maximum near $t = 0$. Too small a noise intensity results in a large number of well-defined peaks; however, the switching frequency drops considerably so that digital simulations take an unacceptable length of time. For the signal and noise values used here, the simulations (carried out on a HP-Apollo DN-425 workstation) took about 36 h to perform and involved 40 000 switching events for each histogram using a step size of 0.001. For simulation purposes, the white noise case corresponds to selecting an integration step size that is much greater than τ_c. For colored noise, τ_c exceeds the step size. Only ISIHs *corresponding to the ABAB symmetry* are considered here.

5.1 Return maps

In the absence of modulation ($\varepsilon = 0$), the simulated ISIHs, and often the neural spontaneous ISIH, are of gamma-type (Sect. 4.1); the dot density in the associated return map (a scatter plot of interval I_{i+1} vs I_i) first increases and then dies off exponentially with distance along the horizontal and vertical directions. Successive intervals are not significantly correlated (in either the $\varepsilon = 0$ or $\varepsilon \neq 0$ case), as lines connecting successive points show no obvious patterns and assume random orientations (not shown). This is also the case for the auditory data of interest here (although nonrenewal properties such as correlations over long time scales or between firing phases have been reported, see, e.g., Lowen and Teich 1992; Longtin 1993). Figure 3b shows a return map of the auditory data used in Fig. 2a. The tendency of the dots to cluster on a lattice with intersections at all integer

multiples of T_0 (= 1.25 ms) indicates the ABAB symmetry. Moreover, there is a definite diagonal symmetry of slope -1 as indicated by the elongations of the individual clusters (this is often seen at frequencies below 1000 Hz). Similar scatter plots (including the elongation of the clusters) are obtained by plotting the successive ISIs from the model data used to generate Fig. 2c (not shown, although similar features appear in Fig. 3d discussed below). The lattice and negatively sloped clusters are thus basic properties of a periodically modulated noisy bistable system. The negative slopes bespeak some form of memory between successive ISIs such that if interval $I_i < mT_0$, then $I_{i+1} > nT_0$, where m, n are integers. Because there is skipping, however, this does not imply a relationship between the duration of successive ISIs. Nevertheless, this noticeable temporal structure is a manifestation of nonrenewal dynamics. This negative slope is enhanced by increasing τ_c as shown in the next section.

5.2 *Effect of the noise correlation time*

This section focusses on the effect of the bandwidth of the noise on the ISIH and return maps. The solid curve of Fig. 3a shows the ISIH from (2) in the quasi-white noise case ($\tau_c = 0.0001$). The striking feature is that, for this soft potential, the dominant peaks lie at $nT_0/2$ with n odd, even though the ABAB symmetry is being considered.

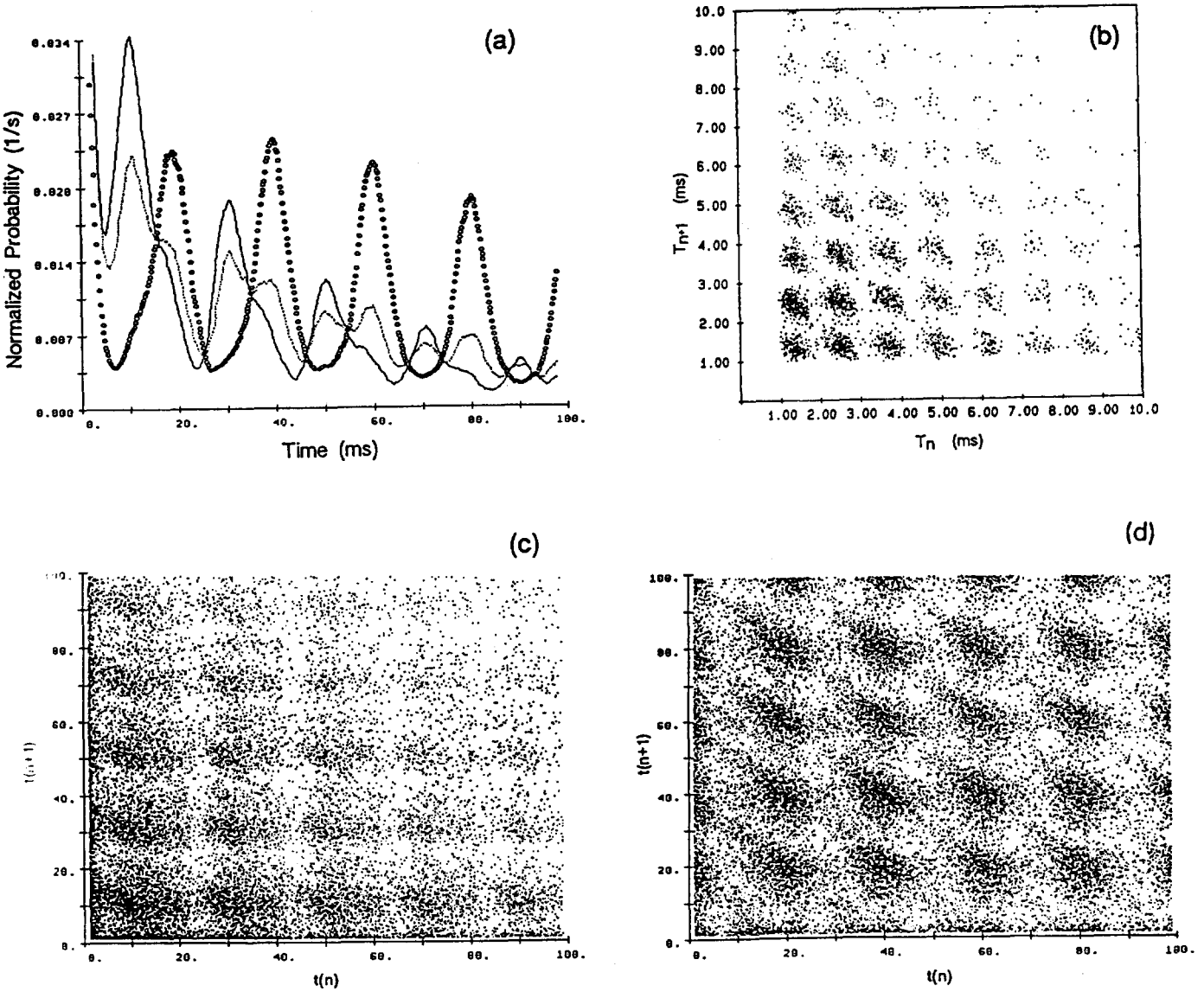

Fig. 3. **a** ISIH from digital simulations of (2) with (b, ε, ω, D) = (1.6056, 0.304, $\pi/10$, 0.067) and $\tau_c = 0.0001$ (*solid curve*), 0.05 (*dotted curve*), and 0.5 (*open circles*). **b** Experimental return map from the cat data used to generate Fig. 2a. **c** Return map corresponding to the ISIH in **a** with $\tau_c = 0.0001$ (quasi-white noise case), for which the points fall within clusters occurring at $nT_0/2$ where n is odd. **d** Same as **c** but with $\tau_c = 0.5$. The clusters occur here at mT_0 where m is an integer

The dotted curve ($\tau_c = 0.05$) shows the peak sequence at $nT_0/2$ with n odd transitioning to the sequence at mT_0 with m an integer; for $\tau_c = 0.5$, the normal ABAB sequence of peaks is recovered. The peaks in the quasi-white case may be explained by observing that, even though the potential is being rocked on a timescale $T_0/2$, there is always a finite probability of $x(t)$ sojourning about the metastable point longer than half a forcing period. A rapid back-and-forth transition at this point will, for example, cut a usual ABAB interval into two smaller ABAB intervals, with the result that the first peak now lies at $T_0/2$. These rapid crossings are emphasized by white noise. The correlations in the noise are passed on to the dynamics of $x(t)$, and the switchings are more compelled to follow the rocking of the potential. Figure 3c shows the associated return map for the quasi-white noise case and Fig. 3d, for the more colored case $\tau_c = 0.5$ (the value of τ_c used for the analog simulations in Fig. 2 are scaled differently than in these digital simulations and is similar to the value used here in the more colored case). The greatest aggregations of points in Fig. 3c are at locations $nT_0/2$ on the time axis, while for the more colored noise case, they occur at locations nT_0. The point clusters are thus seen to gain the negative slope feature as τ_c increases, i.e., as the memory of the noise and thus the autocorrelation of $x(t)$ increases. Finally, the model return maps are mirror symmetric with respect to the $I_{i+1} = I_i$ diagonal because the potential is symmetric about $x = 0$.

Similar results hold if we introduce a coarseness Δt into our measurement of the residence times (or, alternately, a coarseness Δx into our measurement of the position of the particle relative to the barrier). Crossings of the barrier midpoint occurring in rapid succession will then not contribute to ABAB events. Peaks occurring at multiples of $T_0/2$, as seen here for soft potentials (only) with quasi-white noise and/or too finely sampled dynamics, are sometimes observed in the neuron data (Rose et al. 1967; Talbot et al. 1968; Siegel, personal communication). If the neurons reset deterministically, then it is difficult to interpret these "out-of-phase" peaks in the context of a bistable model. On the other hand, our analysis so far has shown that many features of the data can be explained in this context, and it then becomes important to know that different potentials lead to different peak structures. Although the existence of two preferred firing phases (during one cycle), which these peaks imply, has been reported in the auditory literature at higher intensities ("peak splitting", see Johnson 1980), no direct relation to this effect is intended at this time. Also, the number of fast events (in the first bins) decreases as τ_c increases. Accordingly, the ISIH mean increases, implying a decrease in the Kramer's rate, as expected for colored noise (Sect. 3). Finally, in Fig. 3 τ_c was varied without changing D. This implies that the noise power (the integral of the power spectrum, equal to D/τ_c) decreases as τ_c increases. If D is decreased, the peaks are sharper (troughs are lower), and the probability spreads out from the origin to the other peaks (the same effect occurs if ε is decreased). This is difficult to illustrate in practice because low D simulations are prohibitively long to carry out.

5.3 *Scaling of the ISIH decay rate*

Here we investigate the dependence of the ISIH decay rate λ on ε. This rate can be suitably defined when the ISIH is almost exponential (i.e., for higher amplitude or lower frequency stimuli). Figure 4a plots λ as a function of ε at two noise variances D/τ_c. These results are from analog simulations of the Schmitt trigger. The interesting feature is that over a range of amplitudes, λ itself depends sensitively (exponentially) on ε. By comparison, a sensitive power-law-type dependence of λ on ε has been reported in Talbot et al. (1968) and Siegel (1990). Furthermore, we have measured the dependence of λ on D at two values of ε. The results are shown in Fig. 4b and are strikingly similar to those in Fig. 4a. This is not too surprising since the noise and the signal are additive terms on an equal footing in (1). Thus, over a certain range of parameters, noise and signal seem to play interchangeable roles in the determination of ISIH shape. Their roles are not completely reciprocal, however, since peak widths grow with D. It is also interesting to note that the stimulus features are encoded in the ISIH: ω determines the position of the peaks; ε, ω, and D determine the ISIH envelope; and the phase preference is reflected in the width of the peaks. Noise may be used by the neuron to encode the stimulus features in such an ISIH, all the while preserving a fine amplitude discrimination through an exponential dependence of λ on ε.

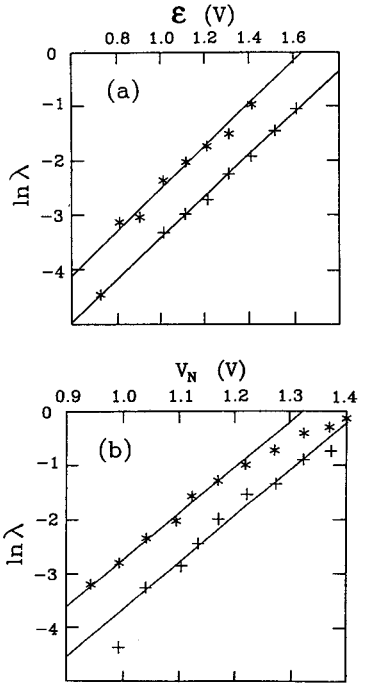

Fig. 4. Log-linear plot of the dependence of the ISIH decay rate on (**a**) ε at two values of D (*: $V_n = 1.0$; + : $V_n = 0.90$) and on (**b**) D at two values of ε (*: $\varepsilon = 1.0$; + : $\varepsilon = 0.80$). The results are obtained from analog simulations on a Schmitt trigger. The value of D is obtained from a measurement of $V_n^2 \equiv \langle V^2(t) \rangle \equiv (D/\tau_c)$ at the output of the noise generator

6 Discussion

Our study has described the features of the ISIH data from sensory neurons which arise from two-state dynamics: the ISIH shape, the return maps, the nonrenewal effects, the noise bandwidth effects, and the scaling of the ISIH decay rate with amplitude. Our results are general and apply to any form of bistability driven by deterministic and stochastic forces, be it in the electrical activity of single cells, cell populations, membrane channels, etc. Whatever the state variable, it is important to realize that the noise may be used advantageously, for example, by enhancing signal detection through stochastic resonance. Our results are also expected to hold when the stimulus is not sinusoidal as e.g., in Siegel's recordings (1990) where the amplitude is driven by a square wave. Our intuition is based on results (e.g., Zheng 1991) which show that SR with nonharmonic forcing can be similar to that with harmonic forcing. It is not known whether, as $\varepsilon \to 0$, the multimodal ISIHs converge to the spontaneous ISIHs in the same way in both the model and the real system. In the context of models described by (1), this would imply that the noise level is input-independent. The spontaneous data were not available at the time of our study, and this question will be pursued elsewhere.

There is a certain symmetry between bistable and IF models. IF models can be deterministic (these can fire periodically), stochastic, or both. In the latter case, the "voltage" performs a random walk with drift to an absorbing barrier, at which point it is reset to a resting value. The barrier of the bistable model is not absorbing, and the particle evolves in a similar potential on the other side of it. The effect of asymmetry, in which the transition back to the resting state is more favorable than the opposite transition, should be investigated (preliminary results indicate no major qualitative differences). A mean first passage time (MFPT) to the absorbing threshold is a natural quantity for the IF model and can be estimated as the ISIH mean. The equivalent quantity for the bistable model is the mean duration of an ABAB event (the ISIH mean also). It is not exact (because of correlation effects) to say that an ABAB event consists of two IF-type events, but the two intervals may be roughly similar. The bistable model also has no absolute refractoriness, since successive crossings of the metastable point arbitrarily close in time can occur (see Sect. 5). However, the noiseless IF model can have absolute refractoriness if there is a drift to threshold. This property disappears as soon as there is noise.

A crucial question is whether, in the presence of a periodic stimulus, the noise is always needed for firings to occur, as it is in our simplified models. The answer may be different for different sensory cells. In fact, skipping is seen over a large range of amplitudes in auditory neurons (Rose et al. 1967), but not in the mechano receptors of the skin (Talbot et al. 1968; Chialvo and Apkarian 1993). In our model, the ISIH collapses quickly to the first peak as deterministic switching becomes possible. Thus, to produce skipping with noisy bistability, the dynamic range of the periodic input to the cell must somehow be compressed to a range near or below the level at which deterministic firing occurs. This may be accomplished by nonlinear compression or by automatic gain control, which in the auditory case could occur at the cochlear mechanics level (see, e.g., Weiss 1966; Lyon 1990). Future investigations will hopefully clarify whether noise is used to enhance signal detection and extend the encoding capabilities in the way our study suggests.

Acknowledgements. We acknowledge helpful discussions with Vania Apkarian, Dante Chialvo, Valerie Gremillion, William Rhode, John Rinzel, Ralph Siegel, and Malvin Teich. Many thanks are due to W. Rhode of the University of Wisconsin for providing the cat auditory data. Support from A.L. from Los Alamos National Laboratory and NSERC (Canada) is gratefully acknowledged. This work was done under the auspices of the National Institute of Mental Health through grant 1-R01-MH47184-01, the Office of Naval Research through grants no. N00014-90-J-1327 and no. N00014-90-AF-001, and the US Department of Energy.

References

Bulsara A, Jacobs E, Zhou T, Moss F, Kiss L (1991) Stochastic resonance in a single neuron model: theory and analog simulation. J Theor Biol 154:531–555

Calvin W, Stevens CF (1968) Synaptic noise and other sources of randomness in motorneuron interspike interval. J Neurophysiol 31:574–587

Chialvo DR, Apkarian V (1993) Modulated noisy biological dynamics: three examples. J Stat Phys 70:375–391

Corey DP, Hudspeth AJ (1983) Kinetics of the receptor current in bullfrog saccular hair cells. J Neurosci 3:962–976

Douglass JK, Moss F, Longtin A (1993) Statistical and dynamical interpretation of ISIH data from periodically stimulated sensory neurons. In: Hanson SJ, Cowan J, Giles L (eds) Proceedings of the fifth neural information processing systems conference, Denver. Morgan Kaufmann, San Francisco

Gammaitoni L, Marchesoni F, Menichella-Saetta E, Santucci S (1989) Stochastic resonance in bistable systems. Phys Rev Lett 62: 349–352

Gardiner C (1983) Handbook of stochastic methods. Springer, Berlin Heidelberg New York

Gerstein GL, Mandelbrot B (1964) Random walk models for the spike activity of a single neuron. Biophys J 4:41–68

Glass L, Graves C, Petrillo GA, Mackey MC (1980) Unstable dynamics of a periodically driven oscillator in the presence of noise. J Theor Biol 86:455–475

Hopfield JJ (1982) Neural networks and physical systems with emergent collective computational abilities. Proc Nat Acad Sci USA 79:2554–2558

Johnson DH (1974) The response of single auditory-nerve fibers in the cat to single tones: synchrony and average discharge rate. PhD thesis, Massachusetts Institute of Technology, Cambridge, Mass

Johnson DH (1980) The relationship between spike rate and synchrony in responses of auditory-nerve fibers to single tones. J. Acoust Soc Am 68:1115–1122

Jung P, Hanggi P, Marchesoni F (1989) Colored-noise-driven bistable systems. Phys Rev A 40:5447–5450

Kiang NYS (1984) Peripheral neural processing of auditory information. In: Handbook of physiology, Vol III. Sensory processes. American Physiological Society, Part 2, Chap 15, pp 639–674

Landahl H, McCulloch WS, Pitts W (1943) A statistical consequence of the logical calculus of nervous nets. Bull Math Biophys 5:135–137

Longtin A (1993a) Stochastic resonance in neuron models. J Stat Phys 70:309–327

Longtin A (1993b) Nonlinear forecasting of spike trains from sensory neurons. Int J Bifurc Chaos (in press)

Longtin A, Bulsara A, Moss F (1991) Time interval sequences in bistable systems and the noise-induced transmission of information by sensory neurons. Phys Rev Lett 67:656–659

Lowen SB, Teich MC (1992) Auditory-nerve action potentials form a nonrenewal point process over short as well as long time scales. J Acoust Soc Am 92:803–806

Lyon RF (1990) Automatic gain control in cochlear mechanics. In: The mechanics and biophysics of hearing. (Lecture notes in biomathematics, Vol 87) pp 395–402

Mannella R, Palleschi V (1989) Fast and precise algorithm for computer simulation of stochastic differential equations. Phys Rev A 40:3381–3386

McNamara B, Wiesenfeld K (1989) Theory of stochastic resonance. Phys Rev A 39:4854–4875

Ogawa T, Bishop PO, Levick WR (1966) Temporal characteristics of responses to photic stimulation by single ganglion cells in the unopened eye of the cat. J Neurophysiol 6:2–30

Rinzel J, Ermentrout B (1989) Analysis of neural excitability and oscillations. In: Koch C, Segev I (eds) Methods in neuronal modeling. MIT Press, Cambridge, Mass

Rose J, Brugge J, Anderson D, Hind J (1967) Phase-locked response to low-frequency tones in single auditory nerve fibers of the squirrel monkey. J Neurophysiol 30:769–793

Russell IJ, Sellick PM (1978) Intracellular studies of hair cells in the mammalian cochlea. J Physiol 284:261–290

Siebert WM (1965) Some implications of the stochastic behavior of primary auditory neurons. Kybernetik 2:206–215

Siegel R (1990) Nonlinear dynamical system theory and primary visual cortical processing. Physica 42 D:385–395

Talbot W, Darian-Smith I, Kornhuber H, Mountcastle V (1968) The sense of flutter-vibration: comparison of the human capacity with response patterns of mechanoreceptive afferents for the monkey hand. J Neurophysiol 31:301–334

Treutlein H, Schulten K (1985) Noise induced limit cycles of the Bonhoeffer-Van der Pol model of neural pulses. Ber Bunsenges Phys Chem 89:710–718

Tuckwell HC (1989) Stochastic processes in the neurosciences. SIAM, Philadelphia

Weiss TF (1966) A model of the peripheral auditory system. Kybernetik 3:153–175

Zheng W (1991) Square-wave-driven stochastic resonance. Phys Rev A 44:6443–6447

Zhou T, Moss F, Jung P (1990) Escape-time distributions of a periodically modulated bistable system with noise. Phys Rev A 42: 3161–3169